

See discussions, stats, and author profiles for this publication at: <https://www.researchgate.net/publication/276065586>

Enhancing Thermal Stability and Lifetime of Solid-State Dye-Sensitized Solar Cells via Molecular Engineering of the Hole-Transporting Material Spiro-OMeTAD

ARTICLE *in* ACS APPLIED MATERIALS & INTERFACES · MAY 2015

Impact Factor: 6.72 · DOI: 10.1021/am5090385 · Source: PubMed

CITATIONS

3

READS

54

9 AUTHORS, INCLUDING:



Tadas Malinauskas

Kaunas University of Technology

44 PUBLICATIONS 271 CITATIONS

[SEE PROFILE](#)



Maryte Daskeviciene

Kaunas University of Technology

21 PUBLICATIONS 98 CITATIONS

[SEE PROFILE](#)



Vytautas Getautis

Kaunas University of Technology

119 PUBLICATIONS 648 CITATIONS

[SEE PROFILE](#)

Enhancing Thermal Stability and Lifetime of Solid-State Dye-Sensitized Solar Cells via Molecular Engineering of the Hole-Transporting Material Spiro-OMeTAD

Tadas Malinauskas,[†] Daiva Tomkute-Luksiene,[†] Rüdiger Sens,[‡] Maryte Daskeviciene,[†] Robert Send,[‡] Henrike Wonneberger,[‡] Vygintas Jankauskas,[§] Ingmar Bruder,^{*,‡} and Vytautas Getautis^{*,†}

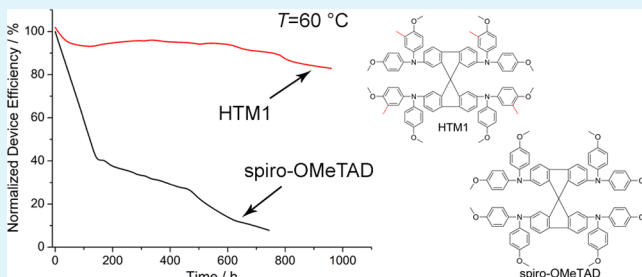
[†]Department of Organic Chemistry, Kaunas University of Technology, Radvilenu pl. 19, Kaunas 50254, Lithuania

[‡]BASF SE, Carl-Bosch-Strasse 38, Ludwigshafen 67056, Germany

[§]Department of Solid State Electronics, Vilnius University, Saulėtekio 9, Vilnius 10222, Lithuania

Supporting Information

ABSTRACT: Thermal stability of hybrid solar cells containing spiro-OMeTAD as hole-transporting layer is investigated. It is demonstrated that fully symmetrical spiro-OMeTAD is prone to crystallization, and growth of large crystalline domains in the hole-transporting layer is one of the causes of solar cell degradation at elevated temperatures, as crystallization of the material inside the pores or on the interface affects the contact between the absorber and the hole transport. Suppression of the crystal growth in the hole-transporting layer is demonstrated to be a viable tactic to achieve a significant increase in the solar cell resistance to thermal stress and improve the overall lifetime of the device. Findings described in this publication could be applicable to hybrid solar cell research as a number of well-performing architectures rely heavily upon doped spiro-OMeTAD as hole-transporting material.



KEYWORDS: charge transport, morphological stability, hybrid solar cells, amorphous materials, spiro compounds

INTRODUCTION

Modern society is facing ever growing concerns over climate change caused by the combustion of fossil fuels.^{1–3} Of the available renewable and clean energy sources, solar energy is the most abundant. Therefore, it is no surprise that there has been a recent surge in the development of photovoltaic technologies.⁴ Photovoltaic devices based on crystalline, inorganic semiconductors have reached impressive power conversion efficiencies of over 28% in single-junction, and 37% in multijunction, device architectures under full-sun illumination.⁵ However, this class of photovoltaics suffers from its high production and energy costs, which result in long financial and energy payback times.^{6–9} This has promoted the development of solution processable solar cells,^{10–13} which benefit from low-cost materials, cheap, high-throughput manufacturing methods and low energy expenditure.¹⁴ The dye-sensitized solar cell (DSSC) has been a long-standing candidate to fulfill this long list of requirements. For the solid-state version (ssDSSC), power conversion efficiencies of over 20% have been predicted,¹⁵ while utilizing low-cost materials,¹⁶ low-temperature processing (<150 °C), and reel-to-reel fabrication methods.^{17,18} However, despite numerous improvements to the electron-transporting anode, the light-absorbing dye sensitizers, and the hole-transporting materials, the ssDSSC

have not fully realized projected potential. The best-performing ssDSSC demonstrated power conversion efficiency of over 7%.¹⁹

Recently, organic–inorganic lead halide perovskite compounds have been utilized as sensitizers in ssDSSC devices. The lead iodide perovskite derivatives have high extinction coefficients, direct bandgaps, large exciton diffusion lengths, and excellent absorption throughout the UV–vis–NIR spectrum.²⁰ In late 2012 lead iodide perovskite ($\text{CH}_3\text{NH}_3\text{PbI}_3$)-sensitized mesoscopic solid solar cells with 2,2',7,7'-tetrakis(*N,N*-di-*p*-methoxyphenylamine)-9,9'-spirobi-fluorene (spiro-OMeTAD) as hole-transporting material (HTM) have been reported to reach 9.7% efficiency.²¹ Subsequent to this discovery, lead halide perovskite based solid-state devices, using spiro-OMeTAD as HTM, have been developing rapidly and an efficiency of 19.3% has been recently reported.²²

To date spiro-OMeTAD is the main, indeed almost the only, organic HTM being extensively studied for application in the perovskite- and dye-sensitized solar cells.^{23–29} With the aid of

Received: December 22, 2014

Accepted: May 8, 2015

Published: May 8, 2015

sophisticated photophysical characterization and theoretical calculations, much of the device optimization work including doping, pore-filling, thickness, and porosity of TiO_2 , and reduction of recombination, is centered on spiro-OMeTAD. While several alternatives have been proposed,^{30–40} spiro-OMeTAD still remains the most widely used and best performing solid-state hole-transporting material.

While all-solid-state hybrid devices have shown substantial improvements in cell performance, surprisingly few studies have been published on their long-term stability.^{19,21,41–45} Most publications about organic and hybrid photovoltaics emphasize device performance, and researchers all over the world are involved in the “efficiency race”. Nevertheless, it will ultimately be their stability (i.e., their lifetime under operation) that will determine whether these device platforms are just interesting photovoltaic concepts or viable technology. Solar cell stability is a measure of whether a given technology can withstand long-term exposure to the conditions relevant to solar cell use, such as high illumination, temperature, or humidity.

The main degradation cause of the HTMs used in perovskite and ssDSSCs photovoltaic devices is probably the oxidation of the hole transporter after prolonged exposure to air.^{32,46–53} As a result, proper encapsulation is absolutely critical for the long-term stability of ssDSSCs. While the oxidation products are stable over the short term, there is a lack of studies on long-term stability of this doping mechanism when the solar cells are exposed to light and increased temperatures in the absence of oxygen. Another stability concern is morphological changes in the HTM upon long exposure to both light and high temperatures. The most common HTMs have been shown to be amorphous,⁵⁴ yet crystallization of the HTM inside the pores or on the interfaces could affect the contact to the light absorber as well as hole transport.

In this publication we have focused our attention on the investigation of the thermal stability of spiro-OMeTAD and its impact on overall device stability under thermal stress. Furthermore, we have studied ways to increase thermal stability of the HTM via the molecular engineering of the HTM.

In light of the atmospheric sensitivity of the perovskite devices, they should be fabricated under controlled atmospheric conditions, with low humidity and with reliable encapsulation.^{55–57} Quality of environmental sealing of the perovskite devices is a very important factor that could significantly influence device lifetime in HTM thermal stability studies. Furthermore, very little is known about the effects of perovskite interaction with the encapsulation material; therefore, we have decided to conduct the experiments with more stable but less efficient ssDSSC.

RESULTS AND DISCUSSION

Morphological Properties of the Spiro-OMeTAD.

Investigation of the pure sample of spiro-OMeTAD, using differential scanning calorimetry (DSC), indicates that the material could exist in both crystalline and amorphous states. During the first scan, only melting of the crystals (T_m) is detected at 245 °C, and no crystallization was observed during the cooling and second heating steps, only the glass transition (T_g) at 124 °C (Figure 1 and Table 1).

The material's behavior under simulated processing conditions was also investigated. The samples of spiro-OMeTAD were placed into the DSC pans, and some of them were heated in an oven under argon atmosphere at 270 °C until the HTM melted to then cool down to room temperature (RT). The

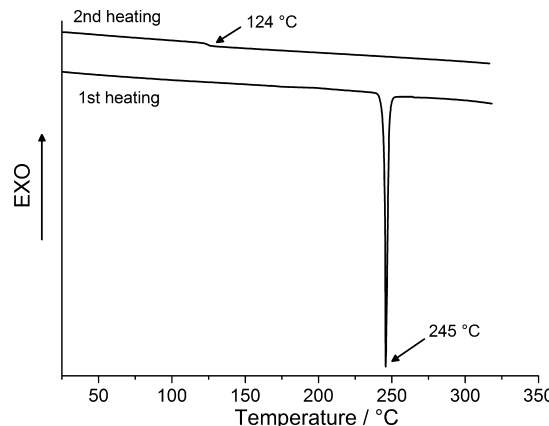


Figure 1. DSC first and second heating curves of spiro-OMeTAD (heating rate 10 °C min⁻¹).

Table 1. Thermal and Photoelectrical Properties of Spiro-OMeTAD and HTM1–HTM3

| compd | T_m (°C) | T_g (°C) | T_{dec} (°C) | I_p^a (eV) | μ_0^b (cm ² V ⁻¹ s ⁻¹) |
|--------------|---------------|---------------|-------------------|----------------------|---|
| spiro-OMeTAD | 245 | 124 | 449 | 5.00 | 4.1×10^{-5} |
| HTM1 | 237 | 121 | 440 | 4.95 | 5.3×10^{-5} |
| HTM2 | 139 | 444 | 5.08 | 4.5×10^{-6} | |
| HTM3 | 135 | 438 | 5.02 | 6×10^{-6} | |

^aIonization potential was measured by the photoemission in air method from films. ^bMobility value at zero field strength.

other set of samples was dissolved in dichloromethane, and placed in an oven under argon atmosphere at 90 °C for 20 min to simulate rapid solvent evaporation from film during spin-coating procedure. The morphological investigation of both sets of the samples was carried out using a DSC analysis (Figure 2 and Table 1).

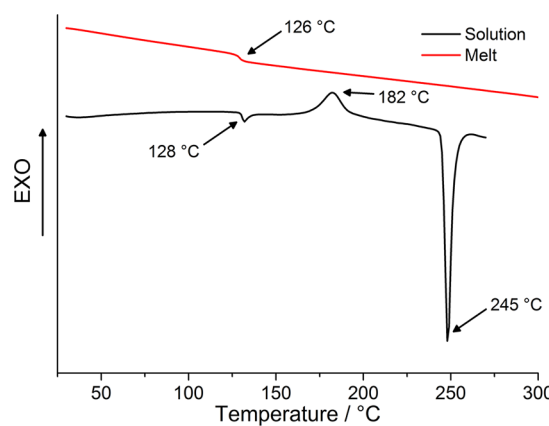


Figure 2. DSC curves of the melted and solution processed samples of the spiro-OMeTAD (heating rate 10 °C min⁻¹).

Interestingly, it was noticed that crystallization from the concentrated DCM solutions could be easily induced upon stirring the dissolved material with a spatula or providing nucleation centers by any other means. DSC analysis confirmed this observation; results for samples prepared from solution look totally different compared to the ones obtained from the melt.

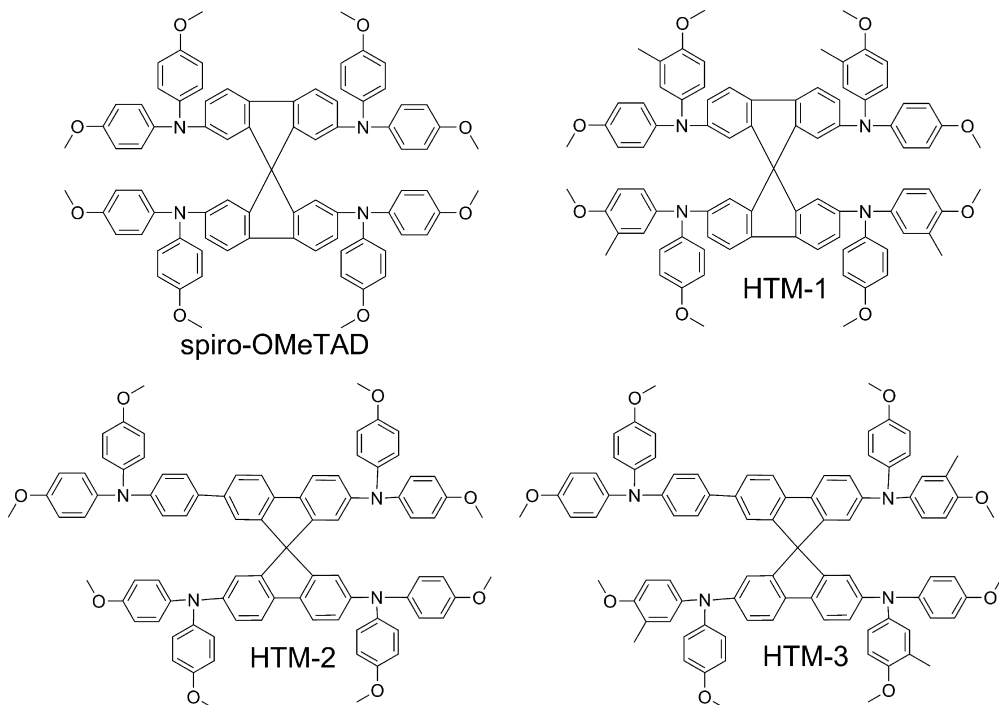


Figure 3. Structures of the synthesized spiro-OMeTAD analogues.

Spiro-OMeTAD remained amorphous upon solidifying from the melt, and only the glass transition temperature was observed. Most likely the viscous nature of the melted material as well as the large size and complex shape of the spiro-OMeTAD prevent a fast orderly arrangement of the molecules and inhibit crystallization. In the solution, on the other hand, movement of the molecules is not constrained as much, and the HTM readily crystallizes. DSC data indicates that samples prepared from solution are a mixture of amorphous and crystalline material. Both glass transition (at 128 °C) and melting of the crystals (at 245 °C) are observed; additionally, crystallization process is detected at 182 °C. Nucleation centers formed during sample preparation obviously promote crystallization of the amorphous material when it liquefies above the glass transition temperature.

It is important to understand the effect of thermal stress on the morphology of the HTM materials, as temperatures reaching 60–80 °C are not that uncommon in real world solar cells, especially in hot climatic conditions. From the conducted experiments it is evident that the amorphous state of spiro-OMeTAD is not as stable as many researchers believed, and under the right circumstances, especially at elevated temperatures, crystallization of the compound is very likely.

In order to better comprehend the effect of uncontrolled crystal growth of spiro-OMeTAD on solar cell performance and lifetime, it is necessary to compare the results with “spiro-like” HTMs possessing a reduced or totally inhibited tendency to crystallize.

Synthesis of the Asymmetric Spiro-OMeTAD Analogues. One of the methods to achieve reduced crystallinity, without too seriously affecting other properties, is introduction of some degree of asymmetry into the molecule. For this purpose 3 new spiro-OMeTAD analogues have been synthesized and investigated.

Molecules of HTM1–HTM3 have a varying degree of asymmetry introduced into them. HTM1 deviates very little

from the original molecular design, with only small local changes in the diphenylamine fragment as is introduced, while HTM2 and HTM3 are progressively more and more asymmetric. The molecular structures of the investigated charge-transporting materials HTM1–HTM3 are presented in Figure 3; the detailed description of the synthesis procedures could be found in the Supporting Information.

Thermal Properties of the Asymmetric Spiro-OMeTAD Analogue. DSC analysis of the synthesized derivatives HTM1–HTM3 has shown that HTM1, similar to spiro-OMeTAD, can exist in both amorphous and crystalline states. However, contrary to spiro-OMeTAD, during the first heating, both glass transition at 120 °C and melting of the crystals at 237 °C are observed (Figure 4).

Similar to the case of spiro-OMeTAD, presence of the crystalline material induces crystallization of the sample above the glass transition temperature, and the crystallization peak

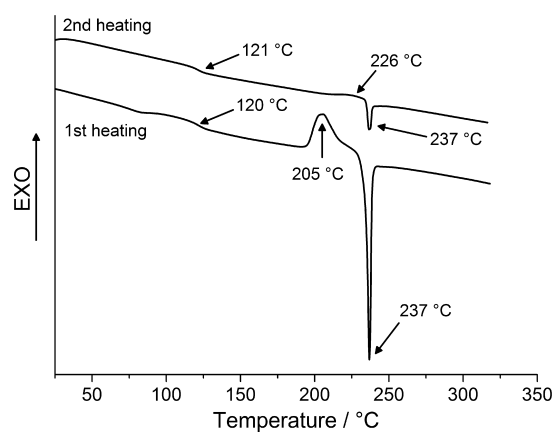


Figure 4. DSC first and second heating curves of HTM1 (heating rate 10 °C min⁻¹).

(T_{cr}) is observed at 205 °C. Interestingly, no crystallization was detected during cooling; however, a small amount of the **HTM1** crystallizes during second heating, although T_{cr} is barely visible and is significantly shifted (by 21 °C) to higher temperature. The intensity of T_m and T_{cr} peaks, as well as the shift of T_{cr} , indicates that the crystallization process is slow and not extensive. The higher degree of asymmetry in **HTM2** and **HTM3** ensures that these two materials remain completely amorphous, and only the glass transition is registered during both heating runs (Figure 5 and Table 1).

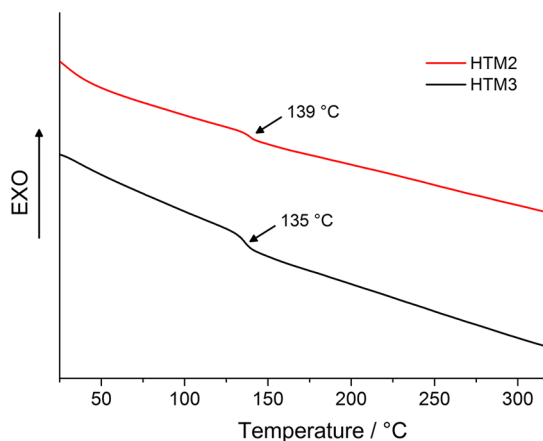


Figure 5. DSC second heating curves of **HTM2** and **HTM3** (heating rate 10 °C min⁻¹).

The influence of the molecular structure on morphological properties of the compounds can be clearly seen from the DSC experiments. Introduction of the methyl group in the diphenylamine fragment of **HTM1** leads to reduction of melting and glass transition temperatures compared with those of spiro-OMeTAD. Increased asymmetry of the molecule, achieved via addition of an extra phenyl ring in **HTM2** and **HTM3**, ensures that both materials remain amorphous. The phenyl ring also adds rigidity to the molecule's core; as a consequence, the glass transition temperature increases by 10–15 °C compared with that of the unmodified spiro-OMeTAD. Similar to the case of **HTM1**, methyl groups reduce the glass transition temperature of **HTM3** by 4 °C, compared with that of **HTM2**.

Thermogravimetry analysis (TGA) revealed that new materials **HTM1**–**HTM3** demonstrate very good thermal stability (Table 1, Supporting Information Figure S1); their decomposition temperatures (T_{dec} 's) ≈ 440 °C are very similar to that of spiro-OMeTAD (449 °C).

Energy Levels, Charge Transport Properties, and Photovoltaic Performance. In a consideration of the use of an organic material for optoelectronic applications, it is important to have an understanding of its solid-state ionization potentials (I_p 's). This understanding can help in identifying a suitable match of organic and inorganic materials. The ionization potential was measured by the electron photoemission in air method (see Supporting Information Figure S2), and results are presented in Table 1; the measurement error is evaluated as 0.03 eV.^{58–60}

Usually the photoemission experiments are carried out in vacuum, and high vacuum is one of the main requirements for these measurements. If the vacuum is not high enough, the sample surface oxidation and gas adsorption are influencing the

measurement results. In our case, however, the organic materials investigated are stable enough to oxygen, and the measurements may be carried out in air. The measured I_p values are very similar for all investigated materials and are close to 5.00 eV. Additional methyl groups in **HTM1** and **HTM3** decrease it slightly by ~0.05 eV, compared with values for spiro-OMeTAD and **HTM2**, while introduction of an extra phenyl ring increases I_p by ~0.08 eV.

Charge transport properties of the synthesized spiro-OMeTAD analogues **HTM1**–**HTM3** were studied by the xerographic time-of-flight (XTOF) technique^{61–63} (see Supporting Information, Figure S3), and values are given in Table 1.

The RT hole-drift mobility of the undoped films of the **HTM1** was $5.3 \times 10^{-5} \text{ cm}^2 \text{ V}^{-1} \text{ s}^{-1}$ at weak electric fields, and it is slightly higher than μ_h of the spiro-OMeTAD. Unfortunately, the charge mobility of **HTM2** and **HTM3** at weak electric fields was approximately 1 order of magnitude lower compared to that of **HTM1** and spiro-OMeTAD. Obviously, the asymmetrical nature of these compounds prevents tight packing, and it is more difficult for the charge to hop between molecules.

Synthesized compounds were tested as hole-transporting materials in ssDSSC in order to evaluate their photovoltaic performance. The J – V characteristics under standard global AM 1.5G solar conditions are shown in Table 2 and Supporting

Table 2. Photovoltaic Performance of ssDSSCs with p-Semiconductors **HTM1–**HTM3**^a**

| compd | J_{SC} (mA cm ⁻²) | V_{OC} (mV) | FF (%) | η (%) |
|--------------|---------------------------------|---------------|------------|----------------|
| spiro-OMeTAD | 9.76 ± 0.4 | 760 ± 20 | 64 ± 1 | 4.8 ± 0.07 |
| HTM1 | 9.34 ± 0.7 | 820 ± 40 | 63 ± 1 | 4.8 ± 0.11 |
| HTM2 | 7.08 ± 0.6 | 800 ± 30 | 38 ± 1 | 2.2 ± 0.10 |
| HTM3 | 7.00 ± 0.4 | 800 ± 20 | 38 ± 1 | 2.1 ± 0.09 |

^aAverage data with standard deviation were based on five cells in a single batch.

Information Figure S4. As expected from the hole mobility measurements, **HTM1** was the best performing new material, and the overall efficiency was identical to that of spiro-OMeTAD. The solar cell performance in the case of compounds **HTM2** and **HTM3** was lower (2.2% and 2.1%, respectively) compared to the device comprising spiro-OMeTAD (4.8%). A decrease in the short-circuit current density in the cases of **HTM2** and **HTM3** most likely could be attributed to the larger charge recombination at HTM/dye interface, which arises from the alterations in the shape of these molecules and subsequent changes in packing and charge transport properties.

Solar Cell Thermal Stability Study. Photovoltaic devices with the investigated HTMs have been subjected to elevated temperatures for prolonged time intervals, and changes in their performance have been monitored. Performances of the solar cells containing spiro-OMeTAD as hole-transporting material have deteriorated rapidly under relatively high thermal stress of 100 °C. In about 250 min the device was no longer functioning (Figure 6).

Microscope pictures of the ssDSSC revealed crystallization of spiro-OMeTAD at elevated temperatures (Figures 6 and 7). As these crystal domains grow ever larger over time, device performance declines to zero. Crystallization of the HTM inside the pores or on the interface most probably affects the contact between the light absorber and the hole transport.^{44,45}

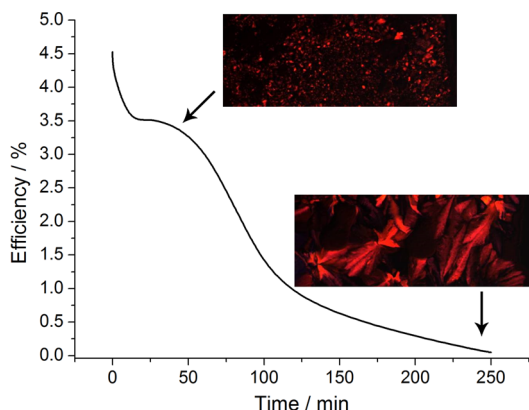


Figure 6. Performance of the spiro-OMeTAD containing ssDSSC heated at 100 °C. Inset shows dark field crossed polarizer microscope pictures of the device.

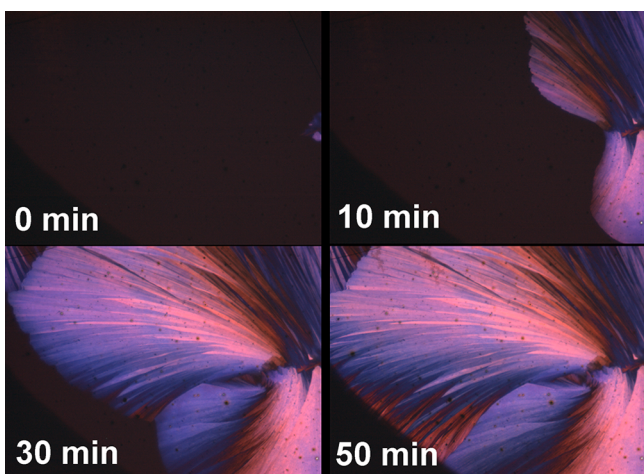


Figure 7. Microscope pictures (dark field crossed polarizers) of the ssDSSC containing spiro-OMeTAD heated at 100 °C.

Under the test conditions, spiro-OMeTAD tends to form large crystalline domains that eventually occupy all of the available area (Figure 7).

Just as DSC experiments have shown, the presence of nucleation centers induces crystallization of the material, and this process is accelerated by elevated temperatures. Mechanical impurities, small crystals that remain if the spiro-OMeTAD is not completely dissolved, or interfaces with other device components can induce crystallization of the HTM. Even thermal evaporation of the metal electrode on top of the hole-transporting material could be a factor catalyzing crystal growth.

In a separate thermal test, designed to demonstrate effects of electrode deposition method upon formation of the crystallization centers, samples of spiro-OMeTAD were spin-coated onto a glass substrate. These samples have crystallized after heating at 200 °C if the silver electrode was evaporated on top. On the other hand, if the HTM material was coated on the glass plate with silver electrodes already present no crystallization was observed under identical testing conditions, even at these high temperatures (Figure 8). These observations correlate with the DSC data (Figures 1 and 2) and indicate that spiro-OMeTAD can remain in an amorphous state even at these relatively high temperatures, provided that no crystal-

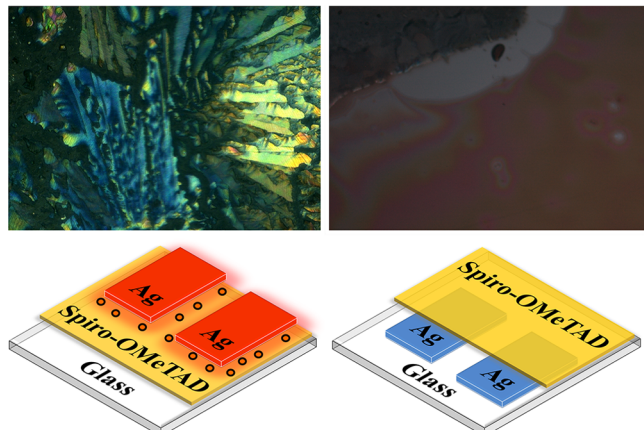


Figure 8. Ag ‘hot’ versus Ag ‘cold’ contact with spiro-OMeTAD (200 °C heating cycle).

lization centers are present, which is very difficult to achieve in a standard solution-based ssDSSC manufacturing process.

Spatially resolved current imaging allows researchers to visually see the effect of crystal growth on the device performance (Figure 9). The bottom right part of the solar

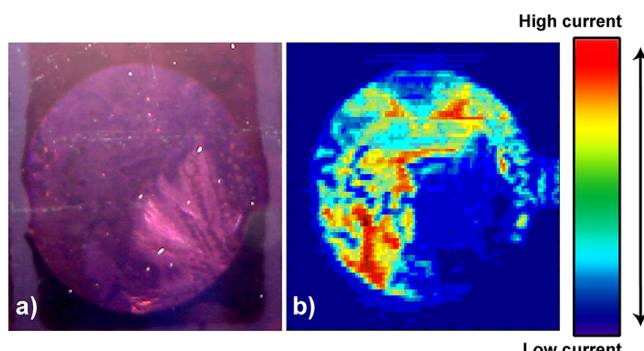


Figure 9. Microscope photo of the crystallization phenomena (a) and spatially resolved current image (b) of the ssDSSC containing spiro-OMeTAD (heated at 100 °C). The solar cell area was illuminated with a laser tip during the current density scanning.

cell, covered by a large crystalline domain of the spiro-OMeTAD, yields much lower currents, compared to the rest of the device. Growth of the large HTM crystals most likely affects the contact to the light absorber and electrode, causing morphological hole traps to form.

Lifetime comparisons of the ssDSSC devices are shown in Figure 10. Not surprisingly, solar cells with spiro-OMeTAD performed the worst; the deterioration process was continuous although not as rapid as in the previous test when higher temperatures (100 °C) were applied.

The fully amorphous spiro analogues **HTM2** and **HTM3** performed significantly better and ~60% of the initial device performance was retained, although a noticeable drop in efficiency is still present. Despite the fact that **HTM1** can be crystalline as well as amorphous, solar cells with **HTM1** demonstrated the best lifetime test results, and only ~10% drop in efficiency was registered after 1000 h at 60 °C. The benefit of the methyl groups, placed at *meta*-position of the phenyl ring in the diphenylamine fragment, could be observed in the cases of both **HTM1** and **HTM3**. It is obvious that even the smallest substituents, placed at correct positions, can make a significant

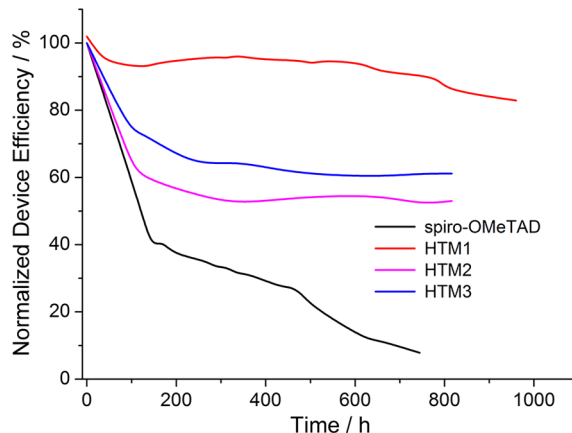


Figure 10. Lifetime of the ssDSSCs comprising hole-transporting materials HTM1– HTM3 and spiro-OMeTAD at 60 °C.

impact on the properties of the compound and subsequent device performance.

Morphological Stability of HTMs with Additives. In order to gain a better understanding of the reasons why **HTM1** performed so well in the lifetime tests we have to look beyond morphological investigations of the pure material and examine a mixture of components that are actually used in solar cell construction. It is a well-known fact that even a small amount of additives, their nature, and the type of the solvent used can have a significant impact on the glass transition, melting, and crystallization temperatures as well as the overall morphological stability of the material in the film of the actual device.

The ~3 μm films, prepared using doctor blade technique, have been dried at 70 °C under Ar atmosphere for 15 min and kept at 100 °C under Ar atmosphere for 1 month. The doctor blade coating technique was chosen purely due to practical reasons as spin-coated films are too thin in order to effectively scrape off 4–5 mg of material for DSC analysis.

Results of the long-term morphological stability test demonstrate that spiro-OMeTAD, similar to the experiments with pristine material, readily crystallizes from the solution (Supporting Information Figure S5, Table 3). **HTM1** on the

Table 3. DSC Results of the Long-Term Morphological Stability Test of the Spiro-OMeTAD and HTM1

| | initial | 1 week | 2 weeks | 3 weeks | 4 weeks |
|---------------------|---------|--------|---------|---------|---------|
| Spiro-OMeTAD | | | | | |
| T _g (°C) | 72 | 110 | 119 | 120 | 122 |
| T _m (°C) | 242 | 243 | 243 | 243 | 243 |
| HTM1 | | | | | |
| T _g (°C) | 66 | 99 | 113 | 119 | 121 |
| T _m (°C) | | | 226 | 229 | 230 |

other hand, does not crystallize as easily, and first signs of crystallization appear after 2 weeks at 100 °C. Looking at the results chart (Figure 11), it is evident that at the beginning of the test glass transition temperatures are dramatically lower, compared with those of pristine materials.

Obviously, liquid tBP (4-*tert*-butylpyridine) and leftover solvent are acting as plasticizers and decrease T_g of the relatively thick films by ~50 °C. Naturally, this value could differ depending on the amount of the tBP used, volatility of the solvent, thickness of the film, and other factors. However, it is clear that the glass transition temperature could be reduced

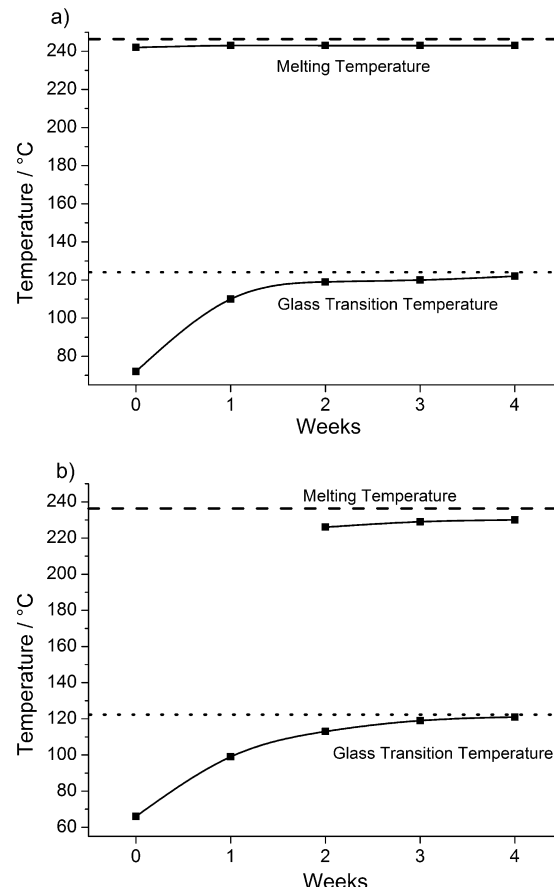


Figure 11. Results chart of the long-term morphological stability test of the spiro-OMeTAD (a) and HTM1 (b). Dotted and dashed lines indicate glass transition and melting temperatures of the pristine sample accordingly.

below 100 °C, which in turn decreases stability of the amorphous state at elevated temperatures.

As the time progresses and volatile components slowly evaporate from the deeper layers of the HTM film, T_g starts to increase, stabilizing around the values recorded for the pristine materials. The evaporation process is quite slow due to the relatively high boiling temperatures of chlorobenzene and especially tBP.⁴⁵ In actual solar cells encapsulation of the device and mesoporous structure of the TiO₂ would prevent or at least severely slow down evaporation and T_g would remain depressed for much longer time periods. Melting temperatures of both HTMs have been slightly decreased due to the presence of the additives.

In order to investigate of the influence of the film thickness on the morphological stability of the HTM layers, ~200 nm spin-coated films, corresponding to the thickness of the material in the actual device, were also prepared and tested under identical conditions.

After 30 days at 100 °C under Ar atmosphere, the X-ray diffraction (XRD) analysis of the doped spiro-OMeTAD samples revealed new features at 5.5°, 5.86°, 6.08°, and 12.16° (Figure 12a), indicating formation of the spiro-OMeTAD crystals in the film. On the other hand, films of the doped **HTM1** did not demonstrate similar changes in the XRD patterns and remained amorphous (Figure 12 b). Thin films used in the morphological stability tests demonstrated no noticeable changes in UV-vis absorption spectra (Supporting

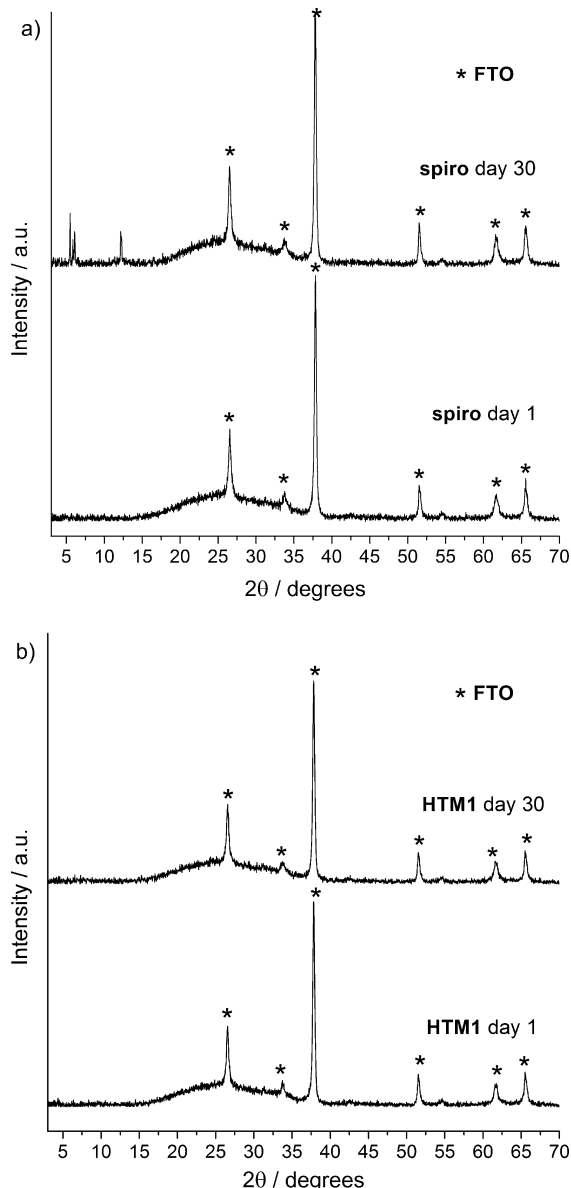


Figure 12. X-ray diffraction spectra of the spiro-OMeTAD (a) and HTM1 (b) films with additives on FTO coated glass substrate.

Information Figure S6) after 30 days at 100 °C, indicating that there were no significant changes in the structure of the doped HTMs.

Influence of the film thickness on the crystallization rate was also investigated using polarized light microscopy, and the results are in good agreement with the DSC and XRD measurements data. Spiro-OMeTAD in thicker films (Supporting Information Figure S7a), formed using the doctor blade technique, crystallizes faster and over a significantly larger area, compared to the thinner spin-coated films (Supporting Information Figure S7c). HTM1, on the other hand, is much less prone to crystallization, and after a month only small separate crystals are observed in thicker films (Supporting Information Figure S7b), while spin-coated ones remained completely unchanged (Supporting Information Figure S7d). From the conducted DSC, XRD, and microscopy measurements it is evident that crystallization processes are noticeably slowed down in thinner films, most likely due to the faster evaporation of the volatile components from thinner ~200 nm

films. As a consequence glass transition temperature stabilizes above 100 °C much more quickly, and the conditions for crystal growth become less favorable. Nevertheless, spiro-MeOTAD starts to crystallize even under these circumstances, while HTM1 remains amorphous. Most likely growth of the large crystals is impaired in HTM1 due to a less orderly structure of the compound, compared with the spiro-OMeTAD. Therefore, the material is morphologically more stable, and the overall lifetime of the devices increases significantly under thermal stress.

CONCLUSIONS

In summary, we have demonstrated that growth of large crystalline domains in the hole-transporting layer is one of the causes of solar cell degradation at elevated temperatures. Most probably, crystallization of the HTM inside the pores or on the interface affects the contact between the light absorber and the hole transport. The fully symmetrical spiro-OMeTAD is prone to crystallization, especially if processed from solution. This process is accelerated by the presence of leftover solvent and liquid additives, such as 4-*tert*-butylpyridine. They act as plasticizers, significantly reducing the glass transition temperature and overall morphological stability of the amorphous state. One of the possible solutions to the problem is the introduction of local asymmetry into the spiro-OMeTAD molecule. This tactic suppresses crystal growth in the HTM layer and significantly increases solar cell resistance to thermal stress and overall lifetime of the device. Devices with HTM1, a spiro-OMeTAD analogue with four additional strategically well-placed methyl groups, have demonstrated significantly improved lifetime at elevated temperatures and retained ~90% of their initial efficiency after 1000 h at 60 °C, while solar cells with spiro-OMeTAD have deteriorated rapidly under identical conditions. Findings described in this publication could be applicable to the hybrid solar cell research as a number of well-performing architectures rely heavily upon doped spiro-OMeTAD as hole-transporting material.

EXPERIMENTAL SECTION

General Methods and Materials. Chemicals were purchased from Sigma-Aldrich and TCI Europe and used as received without further purification. The ¹H and ¹³C NMR spectra were taken on Varian Unity Inova (300 MHz) and Bruker Avance III 400 (400 MHz) spectrometers at RT. All the data are given as chemical shifts in δ (ppm); (CH₃)₄Si (TMS, 0 ppm) was used as an internal standard. The course of the reaction products was monitored by TLC on ALUGRAM SIL G/UV254 plates and developed with I₂ or UV light. Silica gel (grade 9385, 230–400 mesh, 60 Å, Aldrich) was used for column chromatography. Elemental analysis was performed with an Exeter Analytical CE-440 elemental analyzer, model 440 C/H/N/. Differential scanning calorimetry (DSC) was performed on a Q10 calorimeter (TA Instruments) at a scan rate of 10 K min⁻¹ in the nitrogen atmosphere. Thermogravimetry measurements were done on a Q50 thermogravimetric analyzer (TA Instruments) at a scan rate of 10 K min⁻¹ in the nitrogen atmosphere; thermal decomposition temperature was registered at 5% weight loss. The glass transition temperatures for the investigated compounds were determined during the second heating scan. An electrothermal MEL-TEMP capillary melting point apparatus was used for determination of melting points. Thickness of the films was measured using MarSurf WS1 white light interferometer. Optical microscopy experiments were conducted on Olympus BX-41 equipped with QImaging Go-3 camera. The XRD analysis was performed on the D8 Advance diffractometer (Bruker AXS, Karlsruhe, Germany) operating at the tube voltage of 40 kV and tube current of 40 mA. The X-ray beam was filtered with Ni 0.02 mm

filter to select the Cu K α wavelength. Diffraction patterns were recorded in a Bragg–Brentano geometry using a fast counting detector Bruker LynxEye based on silicon strip technology. The specimens were scanned over the range $2\theta = 3\text{--}70^\circ$ at a scanning speed of 6° min^{-1} using a coupled $2\theta/\theta$ scan type.

Ionization Potential Measurement. The solid-state ionization potential of the layers of the synthesized compounds was measured by the electron photoemission in air method.^{58–60} The samples for the ionization potential measurement were prepared by dissolving materials in CHCl₃ and were coated on Al plates precoated with $\sim 0.5 \mu\text{m}$ thick methyl methacrylate and methacrylic acid copolymer adhesive layer. The thickness of the transporting material layer was $0.5\text{--}1 \mu\text{m}$. Usually photoemission experiments are carried out in vacuum, and high vacuum is one of the main requirements for these measurements. If vacuum is not high enough, the sample surface oxidation and gas adsorption are influencing the measurement results. In our case, however, the organic materials investigated are stable enough to oxygen, and the measurements may be carried out in the air. The samples were illuminated with monochromatic light from the quartz monochromator with deuterium lamp. The power of the incident light beam was $(2\text{--}5) \times 10^{-8} \text{ W}$. The negative voltage of -300 V was supplied to the sample substrate. The counter electrode with the $4.5 \times 15 \text{ mm}^2$ slit for illumination was placed at 8 mm distance from the sample surface. The counter electrode was connected to the input of the BK2-16 type electrometer, working in the open input regime, for the photocurrent measurement. The 10^{-15} to 10^{-12} A strong photocurrent was flowing in the circuit under illumination. The photocurrent I is strongly dependent on the incident light photon energy $h\nu$. The $I^{0.5} = f(h\nu)$ dependence was plotted. Usually the dependence of the photocurrent on incident light quanta energy is well-described by linear relationship between $I^{0.5}$ and $h\nu$ near the threshold.^{58,59} The linear part of this dependence was extrapolated to the $h\nu$ axis, and I_p value was determined as the photon energy at the interception point.

Hole-Drift Mobility Measurement. The samples for the hole mobility measurements were prepared by spin-coating the solutions of the synthesized compounds on the polyester films with conductive Al layer. The layer thickness was in the range $5\text{--}10 \mu\text{m}$. The hole-drift mobility was measured by xerographic time-of-flight technique (XTOF).^{61–63} Electric field was created by positive corona charging. The charge carriers were generated at the layer surface by illumination with pulses of nitrogen laser (pulse duration was 2 ns , wavelength 337 nm). The layer surface potential decrease as a result of pulse illumination was up to $1\text{--}5\%$ of initial potential before illumination. The capacitance probe that was connected to the wide frequency band electrometer measured the speed of the surface potential decrease dU/dt . The transit time t_t was determined by the kink on the curve of the dU/dt transient in double logarithmic scale. The drift mobility was calculated by the formula $\mu = d^2/U_0 t_t$, where d is the layer thickness, and U_0 is the surface potential at the moment of illumination.

Device Fabrication and Characterization. A TiO₂ blocking layer was prepared on a fluorine-doped tin oxide (FTO)-covered glass substrate using spray pyrolysis.⁶⁴ Next, a TiO₂ paste (Dyesol), diluted with terpineol, was applied by screen printing, resulting in a film thickness of $1.7 \mu\text{m}$. All films were then sintered for 45 min at 450°C , followed by treatment in a 40 mM aqueous solution of TiCl₄ at 60°C for 30 min , followed by another sintering step. The prepared samples with TiO₂ layers were pretreated with 5 mM solutions of 2-(*p*-butoxyphenyl)acetohydroxamic acid sodium salt in ethanol. The electrodes were then dyed in 0.5 mM dye *N*-(9,9-dimethylfluoren-2-yl)-9,9-dimethyl-*N*-(4-perylenmonooimide-3-ylphenyl)fluoren-2-amine (ID504) solution in CH₂Cl₂. A 200 nm thick layer of hole-transporting material was applied by spin-coating from a solution in chlorobenzene (60 mg mL^{-1}) also containing $25 \mu\text{L mL}^{-1}$ of Li(CF₃SO₂)₂N solution in acetonitrile (stock solution concentration 145 mg mL^{-1}) and $12 \mu\text{L mL}^{-1}$ of tBP. Fabrication of the device was completed by evaporation of 200 nm of silver as the counter electrode. The active area of the ssDSSC was defined by the size of these contacts (0.13 cm^2), and the cells were masked by an aperture of the same area for measurements. The current–voltage characteristics for all cells were measured with a

Keithley 2400 under 1000 W m^{-2} , AM 1.5G conditions (LOT ORIEL 450 W). The scale of the V_{oc} measurement has an accuracy of 20 mV yielding a systematic error margin of $\pm 20 \text{ mV}$. The incident photon to current conversion efficiencies (IPCE) were obtained with an Acton Research Monochromator using additional white background light illumination. Device lifetime tests were conducted on ssDSSC devices that were sealed after fabrication and constantly kept at 60°C and 30% humidity for the duration of the experiment.

Film Preparation for the Long-Term Morphological Stability Test. The investigated charge-transporting materials (spiro-OMeTAD and HTM1) with bis(trifluoromethane) sulfonimide lithium salt (Li-TFSI) and 4-*tert*-butylpyridine (tBP) additives have been dissolved in chlorobenzene and applied onto FTO coated glass substrates using the doctor blade technique. Concentrations of the materials are identical to those used for the construction of ssDSSC devices. Prepared $\sim 3 \mu\text{m}$ films have been dried at 70°C under Ar atmosphere for 15 min and kept at 100°C under Ar atmosphere for 1 month . Every week a sample of HTM was scraped off and investigated using DSC; no encapsulation was used. A sample for initial testing was taken after the drying step. The doctor blade technique was chosen purely due to practical reasons as spin-coated films are too thin in order to effectively scrape off $4\text{--}5 \text{ mg}$ of material for DSC analysis.

For the investigation of the influence of the film thickness on the morphological stability of the HTM layers, $\sim 200 \text{ nm}$ spin-coated films, corresponding to the thickness of the material in the actual device, were also prepared. Thin samples were obtained using the same solvents, materials, additives, and concentrations. They were tested under identical conditions for 1 month and investigated using X-ray diffraction analysis.

ASSOCIATED CONTENT

S Supporting Information

Synthesis procedures; photoemission in air spectra, electric field dependencies of the hole-drift mobilities, and *J*–*V* curves of the solar cells. The Supporting Information is available free of charge on the ACS Publications website at DOI: 10.1021/am5090385.

AUTHOR INFORMATION

Corresponding Authors

*E-mail: ingmar.bruder@basf.com.

*E-mail: vytautas.getautis@ktu.lt.

Author Contributions

The manuscript was written through contributions of all authors. All authors have given approval to the final version of the manuscript.

Notes

The authors declare no competing financial interest.

ACKNOWLEDGMENTS

This research was supported by the European Social Fund under the Global Grant measure (VP1-3.1-ŠMM-07-K 01-078) and BASF SE. We gratefully acknowledge Dr. V. Gaidelis for the help with ionization potential measurements.

REFERENCES

- (1) Oreskes, N. The Scientific Consensus on Climate Change. *Science* **2004**, *306*, 1686.
- (2) Stern, N. *The Economics of Climate Change: The Stern Review*; Cambridge University Press: New York, 2007.
- (3) Anderson, K.; Bows, A. Beyond ‘Dangerous’ Climate Change: Emission Scenarios for a New World. *Philos. Trans. R. Soc., A* **2011**, *369*, 20–44.
- (4) Lewis, N. S.; Nocera, D. G. Powering the planet: chemical challenges in solar energy utilization. *Proc. Natl. Acad. Sci. U.S.A.* **2006**, *103*, 15729–15735.

- (5) Green, M.; Emery, K.; Hishikawa, Y.; Warta, W.; Dunlop, E. Solar Cell Efficiency Tables (Version 41). *Prog. Photovoltaics* **2013**, *21*, 1–11.
- (6) Fthenakis, V. M.; Kim, H. C. Photovoltaics: Life-Cycle Analyses. *Sol. Energy* **2011**, *85*, 1609–1628.
- (7) Alsema, E. A. Energy Pay-Back Time and CO₂ Emissions of PV Systems. *Prog. Photovoltaics* **2000**, *8*, 17–25.
- (8) Fthenakis, V. M.; Kim, H. C.; Alsema, E. Emissions from Photovoltaic Life Cycles. *Environ. Sci. Technol.* **2008**, *42*, 2168–2174.
- (9) Peng, J.; Lu, L.; Yang, H. Review on Life Cycle Assessment of Energy Payback and Greenhouse Gas Emission of Solar Photovoltaic Systems. *Renewable Sustainable Energy Rev.* **2013**, *19*, 255–274.
- (10) Li, G.; Shrotriya, V.; Huang, J.; Yao, Y.; Moriarty, T.; Emery, K.; Yang, Y. High-Efficiency Solution Processable Polymer Photovoltaic Cells by Self-Organization of Polymer Blends. *Nat. Mater.* **2005**, *4*, 864–868.
- (11) McDonald, S.; Konstantatos, G.; Zhang, S.; Cyr, P.; Klem, E.; Levina, L.; Sargent, E. Solution-Processed PbS Quantum Dot Infrared Photodetectors and Photovoltaics. *Nat. Mater.* **2005**, *4*, 138–142.
- (12) Katagiri, H.; Jimbo, K.; Maw, W. S.; Oishi, K.; Yamazaki, M.; Araki, H.; Takeuchi, A. Development of CZTS-Based Thin Film Solar Cells. *Thin Solid Films* **2009**, *517*, 2455–2460.
- (13) Jeong, S.; Lee, B.-S.; Ahn, S.; Yoon, K.; Seo, Y.-H.; Choi, Y.; Ryu, B.-H. An 8.2% Efficient Solution-Processed CuInSe₂ Solar Cell Based on Multiphase CuInSe₂ Nanoparticles. *Energy Environ. Sci.* **2012**, *5*, 7539–7542.
- (14) Krebs, F. C.; Tromholt, T.; Jorgensen, M. Upscaling of Polymer Solar Cell Fabrication Using Full Roll-to-Roll Processing. *Nanoscale* **2010**, *2*, 873–886.
- (15) Snaith, H. Estimating the Maximum Attainable Efficiency in Dye-Sensitized Solar Cells. *Adv. Funct. Mater.* **2010**, *20*, 13–19.
- (16) Hashmi, G.; Miettunen, K.; Peltola, T.; Halme, J.; Asghar, I.; Aitola, K.; Toivola, M.; Lund, P. Review of Materials and Manufacturing Options for Large Area Flexible Dye Solar Cells. *Renewable Sustainable Energy Rev.* **2011**, *15*, 3717–3732.
- (17) Crossland, E.; Noel, N.; Leijtens, T.; Sivaram, V.; Alexander-Webber, J.; Snaith, H. Mesoporous TiO₂ Single Crystals Delivering Enhanced Mobility and Optoelectronic Device Performance. *Nature* **2013**, *493*, 215–219.
- (18) Yamaguchi, T.; Tobe, N.; Matsumoto, D.; Nagai, T.; Arakawa, H. Highly Efficient Plastic-Substrate Dye-Sensitized Solar Cells with Validated Conversion Efficiency of 7.6%. *Sol. Energy Mater. Sol. Cells* **2010**, *94*, 812–816.
- (19) Burschka, J.; Dualeh, A.; Kessler, F.; Baranoff, E.; Cevey-Ha, N.-L.; Yi, C.; Nazeeruddin, M.; Grätzel, M. Tris(2-(1H-pyrazol-1-il)pyridine)Cobalt(III) as p-Type Dopant for Organic Semiconductors and its Application in Highly Efficient Solid-State Dye-Sensitized Solar Cells. *J. Am. Chem. Soc.* **2011**, *133*, 18042–18045.
- (20) Kojima, A.; Teshima, K.; Shirai, Y.; Miyasaka, T. Organometal Halide Perovskites as Visible-Light Sensitizers for Photovoltaic Cells. *J. Am. Chem. Soc.* **2009**, *131*, 6050–6051.
- (21) Kim, H.; Im, J. H.; Lee, C. R.; Lee, K. B.; Moehl, T.; Marchioro, A.; Moon, S. J.; Baker, R. H.; Yum, J. H.; Moser, J. E.; Grätzel, M.; Park, N. G. Lead Iodide Perovskite Sensitized All-Solid-State Submicron Thin Film Mesoscopic Solar Cell with Efficiency Exceeding 9%. *Sci. Rep.* **2012**, *2*, 591.
- (22) Zhou, H.; Chen, Q.; Li, G.; Luo, S.; Song, T.; Duan, H.-S.; Hong, Z.; You, J.; Liu, Y.; Yang, Y. Interface Engineering of Highly Efficient Perovskite Solar Cells. *Science* **2014**, *345*, 542–546.
- (23) Yang, L.; Cappel, U. B.; Unger, E. L.; Karlsson, M.; Karlsson, K. M.; Gabrielsson, E.; Sun, L.; Boschloo, G.; Hagfeldt, A.; Johansson, E. M. J. Comparing Spiro-OMeTAD and P3HT Hole Conductors in Efficient Solid State Dye-Sensitized Solar Cells. *Phys. Chem. Chem. Phys.* **2012**, *14*, 779–789.
- (24) Jiang, X.; Karlsson, K. M.; Gabrielsson, E.; Johansson, E. M. J.; Quintana, M.; Karlsson, M.; Sun, L.; Boschloo, G.; Hagfeldt, A. Highly Efficient Solid-State Dye-Sensitized Solar Cells Based on Triphenylamine Dyes. *Adv. Funct. Mater.* **2011**, *21*, 2944–2952.
- (25) Cai, N.; Moon, S.-J.; Cevey-Ha, L.; Moehl, T.; Humphry-Baker, R.; Wang, P.; Zakeeruddin, S. M.; Grätzel, M. An Organic D-π-A Dye for Record Efficiency Solid-State Sensitized Heterojunction Solar Cells. *Nano Lett.* **2011**, *11*, 1452–1456.
- (26) Snaith, H. J.; Grätzel, M. Electron and Hole Transport Through Mesoporous TiO₂ Infiltrated with Spiro-MeOTAD. *Adv. Mater.* **2007**, *19*, 3643–3647.
- (27) Liu, M.; Johnston, M. B.; Snaith, H. J. Efficient Planar Heterojunction Perovskite Solar Cells by Vapour Deposition. *Nature* **2013**, *501*, 395–398.
- (28) Lee, M. M.; Teuscher, J.; Miyasaka, T.; Murakami, T. N.; Snaith, H. J. Efficient Hybrid Solar Cells Based on Meso-Superstructured Organometal Halide Perovskites. *Science* **2012**, *338*, 643–647.
- (29) Noh, J. H.; Jeon, N. J.; Choi, Y. C.; Nazeeruddin, M. K.; Grätzel, M.; Seok, S. I. Nanostructured TiO₂/CH₃NH₃PbI₃ Heterojunction Solar Cells Employing Spiro-OMeTAD/Co-Complex as Hole-Transporting Material. *J. Mater. Chem. A* **2013**, *1*, 11842–11847.
- (30) Kroese, J. E.; Hirata, N.; Schmidt-Mende, L.; Orizu, C.; Ogier, S. D.; Carr, K.; Grätzel, M.; Durrant, J. R. Parameters Influencing Charge Separation in Solid-State Dye-Sensitized Solar Cells Using Novel Hole Conductors. *Adv. Funct. Mater.* **2006**, *16*, 1832–1838.
- (31) Snaith, H. J.; Zakeeruddin, S. M.; Wang, Q.; Pechy, P.; Grätzel, M. Dye-Sensitized Solar Cells Incorporating a “Liquid” Hole-Transporting Material. *Nano Lett.* **2006**, *6*, 2000–2003.
- (32) Abrusci, A.; Ding, I.-K.; Al-Hashimi, M.; Segal-Peretz, T.; McGehee, M. D.; Heeney, M.; Frey, G. L.; Snaith, H. J. Facile Infiltration of Semiconducting Polymer Into Mesoporous Electrodes for Hybrid Solar Cells. *Energy Environ. Sci.* **2011**, *4*, 3051–3058.
- (33) Leijtens, T.; Ding, I.-K.; Giovenzana, T.; Bloking, J. T.; McGehee, M. D.; Sellinger, A. Hole Transport Materials with Low Glass Transition Temperatures and High Solubility for Application in Solid-State Dye-Sensitized Solar Cells. *ACS Nano* **2012**, *6*, 1455–1462.
- (34) Hsu, C.-Y.; Chen, Y.-C.; Lin, R. Y. -Y.; Ho, K.-C.; Lin, J. T. Solid-State Dye-Sensitized Solar Cells Based on Spirofluorene (Spiro-OMeTAD) and Arylamines as Hole Transporting Materials. *Phys. Chem. Chem. Phys.* **2012**, *14*, 14099–14109.
- (35) Sepehrifard, A.; Kamino, B. A.; Bender, T. P.; Morin, S. Siliconized Triarylaminies as Redox Mediator in Dye-Sensitized Solar Cells. *ACS Appl. Mater. Interfaces* **2012**, *4*, 6211–6215.
- (36) Grancini, G.; Kumar, R. S. S.; Abrusci, A.; Yip, H.-L.; Li, C.-Z.; Jen, A.-K. Y.; Lanzani, G.; Snaith, H. J. Boosting Infrared Light Harvesting by Molecular Functionalization of Metal Oxide/Polymer Interfaces in Efficient Hybrid Solar Cells. *Adv. Funct. Mater.* **2012**, *22*, 2160–2166.
- (37) Planells, M.; Abate, A.; Hollman, D. J.; Stranks, S. D.; Bharti, V.; Gaur, J.; Mohanty, D.; Chand, S.; Snaith, H. J.; Robertson, N. Diacetylene Bridged Triphenylamines as Hole Transport Materials for Solid State Dye Sensitized Solar Cells. *J. Mater. Chem. A* **2013**, *1*, 6949–6960.
- (38) Yang, L.; Xu, B.; Bi, D.; Tian, H.; Boschloo, G.; Sun, L.; Hagfeldt, A.; Johansson, E. M. J. Initial Light Soaking Treatment Enables Hole Transport Material to Outperform Spiro-OMeTAD in Solid-State Dye-Sensitized Solar Cells. *J. Am. Chem. Soc.* **2013**, *135*, 7378–7385.
- (39) Li, H.; Fu, K.; Hagfeldt, A.; Grätzel, M.; Mhaisalkar, S. G.; Grimsdale, A. C. A Simple 3,4-Ethylenedioxythiophene Based Hole-Transporting Material for Perovskite Solar Cells. *Angew. Chem., Int. Ed.* **2014**, *53*, 4085–4088.
- (40) Jeon, N. J.; Lee, J.; Noh, J. H.; Nazeeruddin, M. K.; Grätzel, M.; Seok, S. I. Efficient Inorganic–Organic Hybrid Perovskite Solar Cells Based on Pyrene Arylamine Derivatives as Hole-Transporting Materials. *J. Am. Chem. Soc.* **2013**, *135*, 19087–19090.
- (41) Wang, M.; Moon, S.-J.; Xu, M.; Chittibabu, K.; Wang, P.; Cevey-Ha, N.-L.; Humphry-Baker, R.; Zakeeruddin, S. M.; Grätzel, M. Efficient and Stable Solid-State Dye-Sensitized Solar Cells Based on a High-Molar-Extinction-Coefficient Sensitizer. *Small* **2010**, *6*, 319–324.
- (42) Chen, C.-Y.; Wang, M.; Li, J.-Y.; Pootrakulchote, N.; Al-Ibabaei, L.; Ngoc-le, C.-H.; Decoppet, J.-D.; Tsai, J.-H.; Grätzel, C.; Wu, C.-G.;

- Zakeeruddin, S. M.; Grätzel, M. Highly Efficient Light-Harvesting Ruthenium Sensitizer for Thin-Film Dye-Sensitized Solar Cells. *ACS Nano* **2009**, *3*, 3103–3109.
- (43) Docampo, P.; Snaith, H. J. Obviating the Requirement for Oxygen in SnO₂-Based Solid-State Dye-Sensitized Solar Cells. *Nanotechnology* **2011**, *22*, 225403.
- (44) Docampo, P.; Guldin, S.; Leijtens, T.; Noel, N. K.; Steiner, U.; Snaith, H. J. Lessons Learned: from Dye-Sensitized Solar Cells to All-Solid-State Hybrid Devices. *Adv. Mater.* **2014**, *26*, 4013–4030.
- (45) Bailie, C. D.; Unger, E. L.; Zakeeruddin, S. M.; Grätzel, M.; McGehee, M. D. Melt-Infiltration of Spiro-OMeTAD and Thermal Instability of Solid-State Dye-Sensitized Solar Cells. *Phys. Chem. Chem. Phys.* **2014**, *16*, 4864–4870.
- (46) Krebs, F. C.; Spanggaard, H. Significant Improvement of Polymer Solar Cell Stability. *Chem. Mater.* **2005**, *17*, 5235–5237.
- (47) Jorgensen, M.; Norrman, K.; Krebs, F. C. Stability/Degradation of Polymer Solar Cells. *Sol. Energy Mater. Sol. Cells* **2008**, *92*, 686–714.
- (48) Leijtens, T.; Lim, J.; Teuscher, J.; Park, T.; Snaith, H. J. Charge Density Dependent Mobility of Organic Hole-Transporters and Mesoporous TiO₂ Determined by Transient Mobility Spectroscopy: Implications to Dye-Sensitized and Organic Solar Cells. *Adv. Mater.* **2013**, *25*, 3227–3233.
- (49) Kruger, J.; Plass, R.; Cevey, L.; Piccirelli, M.; Grätzel, M.; Bach, U. High Efficiency Solid-State Photovoltaic Device Due to Inhibition of Interface Charge Recombination. *Appl. Phys. Lett.* **2001**, *79*, 2085.
- (50) Snaith, H. J.; Grätzel, M. Enhanced Charge Mobility in a Molecular Hole Transporter Via Addition of Redox Inactive Ionic Dopant: Implication to Dye-Sensitized Solar Cells. *Appl. Phys. Lett.* **2006**, *89*, 262114.
- (51) Abate, A.; Leijtens, T.; Pathak, S.; Teuscher, J.; Avolio, R.; Errico, M. E.; Kirkpatrick, J.; Ball, J. M.; Docampo, P.; McPherson, I.; Snaith, H. J. Lithium Salts as “Redox Active” p-Type Dopants for Organic Semiconductors and Their Impact in Solid-State Dye-Sensitized Solar Cells. *Phys. Chem. Chem. Phys.* **2013**, *15*, 2572–2579.
- (52) Cappel, U. B.; Daeneke, T.; Bach, U. Oxygen-Induced Doping of Spiro-MeOTAD in Solid-State Dye-Sensitized Solar Cells and its Impact on Device Performance. *Nano Lett.* **2012**, *12*, 4925–4931.
- (53) Fantacci, S.; De Angelis, F.; Nazeeruddin, M. K.; Grätzel, M. Electronic and Optical Properties of the Spiro-MeOTAD Hole Conductor in its Neutral and Oxidized Forms: a DFT/TDDFT Investigation. *J. Phys. Chem. C* **2011**, *115*, 23126–23133.
- (54) Bach, U.; Lupo, D.; Comte, P.; Moser, J. E.; Weissörtel, F.; Salbeck, J.; Spreitzer, H.; Grätzel, M. Solid-State Dye-Sensitized Mesoporous TiO₂ Solar Cells with High Photon-To-Electron Conversion Efficiencies. *Nature* **1998**, *395*, 583–585.
- (55) Gao, P.; Grätzel, M.; Nazeeruddin, M. K. Organohalide Lead Perovskites for Photovoltaic Applications. *Energy Environ. Sci.* **2014**, *7*, 2448–2463.
- (56) Matteocci, F.; Razza, S.; Di Giacomo, F.; Casaluci, S.; Mincuzzi, G.; Brown, T. M.; D’Epifanio, A.; Licoccia, S.; Di Carlo, A. Solid-State Solar Modules Based on Mesoscopic Organometal Halide Perovskite: a Route Towards the Up-Scaling Process. *Phys. Chem. Chem. Phys.* **2014**, *16*, 3918–3923.
- (57) Niu, G.; Li, W.; Meng, F.; Wang, L.; Dong, H.; Qiu, Y. Study on the Stability of CH₃NH₃PbI₃ Films and the Effect of Post-Modification by Aluminum Oxide in All-Solid-State Hybrid Solar Cells. *J. Mater. Chem. A* **2014**, *2*, 705–710.
- (58) Kirkus, M.; Tsai, M. H.; Grazulevicius, J. V.; Wu, C. C.; Chi, L. C.; Wong, K. T. New Indole-Carbazole Hybrids as Glass-Forming High-Triplet-Energy Materials. *Synth. Met.* **2009**, *159*, 729–734.
- (59) Miyamoto, E.; Yamaguchi, Y.; Yokoyama, M. Ionization Potential of Organic Pigment Film by Atmospheric Photoelectron Emission Analysis. *Electrophotography* **1989**, *28*, 364–370.
- (60) Cordona, M.; Ley, L. Photoemission in Solids I. *Top. Appl. Phys.* **1978**, *26*, 1.
- (61) Montrimas, E.; Gaidelis, V.; Pazera, A. The Discharge Kinetics of Negatively Charged Se Electrophotographic Layers. *Lith. J. Phys.* **1966**, *6*, 578–585.
- (62) Vaezi-Nejad, S. M. Xerographic Time of Flight Experiment for the Determination of Drift Mobility in High Resistivity Semiconductors. *Int. J. Electron.* **1987**, *62*, 361–384.
- (63) Archie, Y.; Chan, C.; Juhasz, C. Xerographic-Mode Transient Charge Technique for Probing Drift Mobility in High-Resistivity Materials. *Int. J. Electron.* **1987**, *62*, 625–632.
- (64) Peng, B.; Jungmann, G.; Jager, C.; Haarer, D.; Schmidt, H. W.; Thelakkat, M. Systematic Investigation of the Role of Compact TiO₂ Layer in Solid State Dye-Sensitized TiO₂ Solar Cells. *Coord. Chem. Rev.* **2004**, *248*, 1479–1489.